Hindawi
Shock and Vibration
Volume 2019, Article ID 1691582, 13 pages
https://doi.org/10.1155/2019/1691582

Research Article

Response of a Two-Degree-of-Freedom Vibration System with Rough Contact Interfaces

Zhiqiang Huang,[1] Xun Peng ,[1] Gang Li,[1] and Lei Hao[2]

[1]*Electromechanical Engineering College, Southwest Petroleum University, Chengdu, Sichuan 610500, China*
[2]*Bureau of Geophysical Prospecting, China National Petroleum Corporation, Zhuozhou, Hebei 072750, China*

Correspondence should be addressed to Xun Peng; px_swpu@foxmail.com

Received 14 August 2018; Accepted 20 January 2019; Published 14 February 2019

Academic Editor: Huu-Tai Thai

This paper is focused on the influence of the rough contact interfaces on the dynamics of a coupled mechanical system. For this purpose, a two-degree-of-freedom model of a coupled seismic-vibrator-rough-ground system is proposed with which the nonlinear vibration properties are analyzed. In this model, the force-deflection characteristic of the contact interfaces is determined by finite element analysis. By analyzing the undamped free vibration, it was found that the variation of the second-order natural frequency with amplitude increases with rougher contact interfaces; however, the amplitude has little influence on the first-order natural frequency of the system. For the harmonic excited analysis, the jump frequencies and hysteretic region both decrease with rougher contact interfaces. Moreover, it is inferred from the bifurcation diagrams that, increasing the excitation force, the system can bring about chaotic motions on rough contact interfaces.

1. Introduction

Contact interfaces exist in a wide range of mechanical systems and play an important role in the overall static and dynamic characteristics of such systems. The rough surface topography of the contact interfaces affects the wear, friction, and normal contact stiffness of the contact mechanics, which has a great influence on the dynamic properties, vibration noise, and energy transfer of the whole mechanical system [1–3]. In order to describe the rough contact interfaces, the fractal geometry is applied to construct the rough surface topography [4, 5]. Berry and Lewis [6] formed the initial basis for a fractal surface roughness description using the Weierstrass–Mandelbrot fractal function. Then, Majumdar and Bushan [7] developed the first-contact models (the MB model) for the rough surface using the Weierstrass–Mandelbrot function. For the last twenty years, analytical approach has been of interest to many researchers. Ciavarella et al. [8] applied the fractal model for the investigation of contact stiffness and contact resistance of rough surfaces. Yan and Komvopoulos [9] extended the MB model to three-dimensional fractal surface and investigated the actual contact area and interfacial contact force of elastic-plastic rough surface. Several researchers have undertaken the study of the normal contact stiffness of rough surfaces [10, 11]. To further consider the impact of friction on the normal contact stiffness, Liu et al. [12] introduced a friction factor into the contact model of elastic-plastic rough surfaces. Due to the shortcomings of analytical approach, such as neglecting the bulk deformation, the finite element analysis has become an efficient way of contact analysis. For example, Komvopoulos et al. [13], Pei et al. [14], and Sahoo et al. [15] adopted finite element analysis for contact between rough surfaces.

Hertzian contact theory is generally employed for modeling the dynamic contact interactions. Nayak [16] introduced a theoretical groundwork to study dynamic contact interactions based on a single-degree-of-freedom (SDOF) system model by using the harmonic balance method. After that, several researchers studied the vibration characteristics of sphere-plane contact [17–20], but such contacts cannot reflect the actual topography of a rough surface. To construct the actual contact interfaces of rough surfaces, Xiao et al. [21]

studied the force-deflection characteristics of a rough solid body-rigid flat surface model and analyzed the free vibration and forced damped vibration of the SDOF system. Tamonash et al. [22] studied how the material properties of rough surfaces influence the force-deflection curves and vibration characteristics of a rough contact system. All the above studies involving SDOF systems are limited to ignore effects of contact interfaces on coupled mechanical system. Two-degree-of-freedom (TDOF) systems are important in engineering analysis because many practical mechanical components involve coupled vibrating systems that can be modeled using TDOF systems [23–25].

To investigate the influence of rough contact interfaces on engineering components, the present investigation takes as its example a seismic vibrator, which is a typical TDOF system. Castanet and Sallas et al. [26, 27] proposed the weighted-sum theory by assuming the vibrator as a TDOF system. After that, several researchers studied the dynamic response of the vibrator by describing it as a TDOF system. Lebedev et al. [28] analyzed the radiation of seismic waves by proposing a theoretical model to account for the baseplate flexure. Liu et al. [29] established the kinetic equations of the vibrator-ground coupled system based on the theory of soil dynamics and analyzed the influence of the system parameters on the vibrator output signal. In its working process, the vibrator radiates signals into the earth by being in contact with the ground surface. Hence, the contact interfaces have important effects on the dynamic response of the vibrator. However, the previous studies lack the influence of the ground surface topography on the free and forced vibrations of the vibrator system, making it necessary to establish a vibrator-rough ground coupled system.

The aim of the present investigation is to study the nonlinear dynamic behavior of a TDOF vibration system that accounts for the influence of rough contact interfaces. As a typical TDOF system, how the contact interfaces influence the free vibrations and damped forced vibrations of the seismic vibrator are analyzed. A modified two-variable Weiestrass–Mandelbrot fractal function is used to construct the ground surface topographies, and the force-deflection characteristic of the vibrator in contact with the rough ground is determined by finite element contact analysis. The power-law function determined by the force-deflection relationship is used to describe the nonlinear contact stiffness between the vibrator and ground. A nondimensional kinetic equation of the TDOF system is developed to study the effect of the rough contact interfaces on the vibration response, and a field experiment is carried out to verify the dynamic model. By using numerical methods, the natural frequency, frequency response, and bifurcation diagram for different rough surface topographies are illustrated. The present research results will assist the study of the effects of contact interfaces on the engineering mechanical systems.

2. Description of the TDOF System

The vibrator is the key component in the seismic vibrators that are used widely in oil and gas exploration. The geometry of the vibrator is shown in Figure 1, the main components of which are the reaction mass and the baseplate (including top plate, supporting columns, piston, and baseplate pad). The reaction mass surrounds the piston, and the weight of former supported by two air suspensions is loaded on the baseplate as a static pressure. When the vibrator is in operation, the vehicle is lifted up and its weight (the hold-down load) is loaded on the vibrator baseplate. The vibrator radiates signals into the earth by being in contacting with the ground; therefore, the vibrator and ground constitute a coupled TDOF system, as shown in Figure 2.

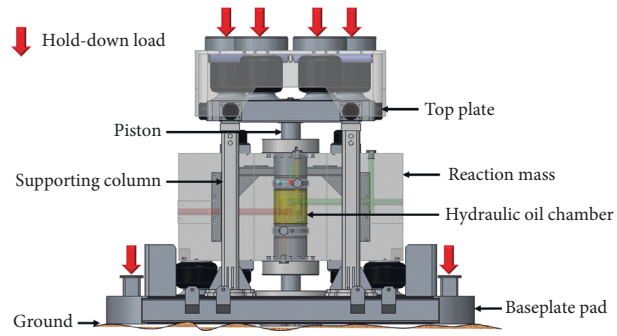

Figure 1: Geometry of the vibrator.

To consider the nonlinear contact characteristics of rough surfaces, a restoring force given by $f(z)$ is applied to the system. The kinetic equation about the static equilibrium position of the TDOF system in Figure 2 is given by

$$\begin{cases} m_1\ddot{z}_1 + d_1(\dot{z}_1 - \dot{z}_2) + k_1(z_1 - z_2) = -F\sin(\omega t), \\ m_2\ddot{z}_2 + (d_1 + d_2)\dot{z}_2 - d_1\dot{z}_1 + f(z_2 + z_{s2}) - F_t \\ \quad - k_1(z_1 - z_2) = F\sin(\omega t), \end{cases} \tag{1}$$

where m_1 is the mass of the reaction mass, m_2 is the mass of the baseplate, z_1 and z_2 are the vibration displacements, k_1 is the hydraulic stiffness, d_1 and d_2 are the linear damping coefficients of the hydraulic oil and the ground, respectively, F_t is the static load, including the hold-down load and the weight of the vibrator, z_{s2} is the static displacement due to the static load, and $F\sin(\omega t)$ is the excitation force.

3. Model and Verification

3.1. Fractal Surface Modeling. To establish the contact interfaces between the vibrator and ground, it is necessary to construct the surface topography of ground. Due to the self-similarity and scale-dependence of the ground surface, a fractal model can be used to describe the surface geometry [30, 31]. The three-dimensional modified ground surface topography is characterized using a modified two-variable Weierstrass–Mandelbrot fractal function [7] given by

$$z(x,y) = L\left(\frac{G}{L}\right)^{(D-2)}\left(\frac{\ln\gamma}{M}\right)\sum_{m=1}^{M}\sum_{n=0}^{n_{\max}}\gamma^{(D-3)n} \cdot \left\{\cos\phi_{m,n} - \cos\left[\frac{2\pi\gamma^n\left(x^2+y^2\right)^{1/2}}{L} \cdot \cos\left[\tan^{-1}\left(\frac{y}{x}\right) - \frac{\pi m}{M}\right] + \phi_{m,n}\right]\right\}, \tag{2}$$

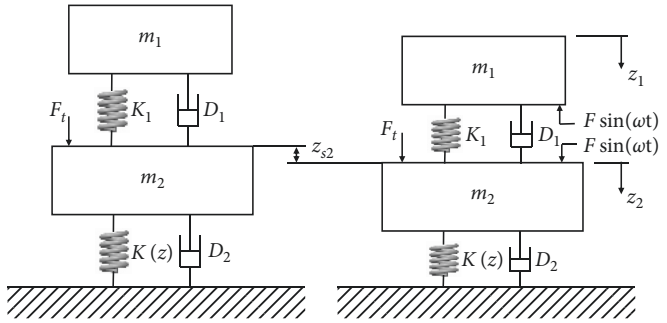

Figure 2: Dynamic model of the vibrator.

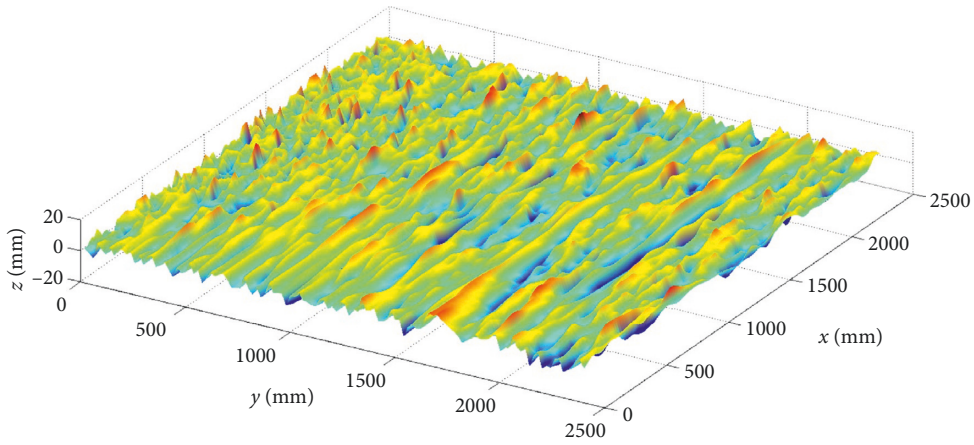

Figure 3: Fractal surface model for $D = 4$, $G = 6e - 4$ m, $L = 2.4$ m, $M = 10$, and $\gamma = 1.5$.

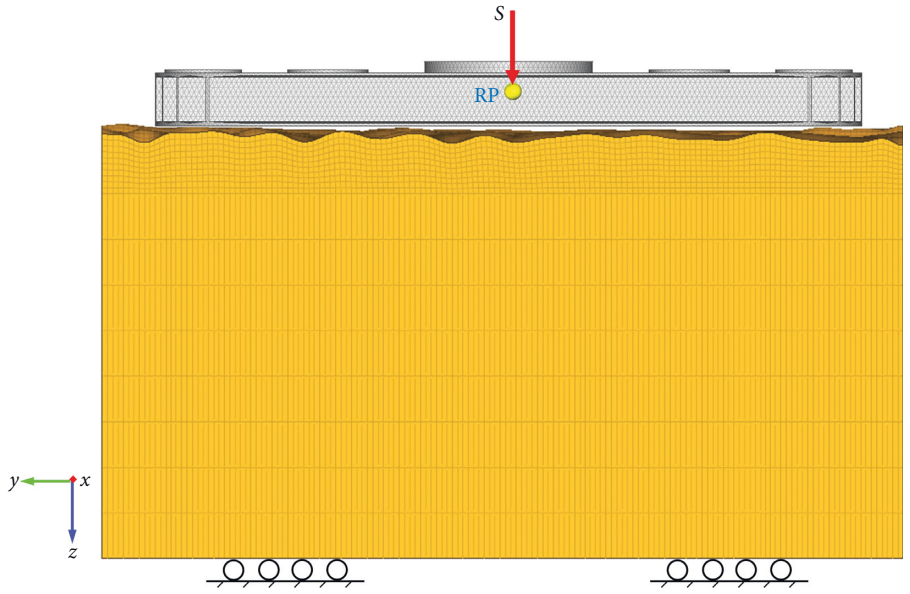

Figure 4: Finite element model of the contact interfaces.

where L is the sample length, D is the fractal dimension that determines the relative contributions of the high and low-frequency components of the surface profile, G is a characteristic length scale of the surface that is independent of the frequency, M is the number of superposed ridges used to construct the surfaces, n is a frequency index ($n_{\max} = \text{int}[\log(L/L_s)/\log\gamma]$), $\phi_{m,n}$ is a random phase in the range $[0, 2\pi]$, and γ ($\gamma > 1$) is a scaling parameter. Consideration regarding surface flatness and frequency distribution density suggests that $\gamma = 1.5$ is

(a) (b)

Figure 5: Field test of the vibrator: (a) the EV56 vehicle; (b) accelerometer located on the reaction mass.

typical for most surfaces [32]. The ground surface height $z(x, y)$ at different points can be evaluated in MATLAB, as shown in Figure 3.

3.2. Finite Element Contact Model. To determine the normal contact stiffness between the contact interfaces, static analysis of rigid flat pad-rough surface is carried out using finite element contact analysis. Because the vibrator is in contact with the rough ground through its baseplate pad, a rough surface with sufficient area for the contact of the baseplate pad must be constructed, and the surface heights were generated from Equation (1) in MATLAB. The surface points were then imported into ABAQUS, and a rough deformable solid body was generated with the generated rough surface profile. The rough ground solid body was meshed using 3D solid element C3D8R, and the mesh size was refined in and near the contact region. The contact interaction between the rough ground and the baseplate was surface-to-surface contact, and the rough surface of the ground solid was defined as the slave surface while the bottom surface of the baseplate pad was the defined as master surface. The bottom of the ground solid was constrained from moving in any directions. The baseplate pad was defined as a rigid body, the centroid of which was chosen as the reference point. As shown in Figure 4, a displacement in the z direction was applied to the reference point to move the baseplate pad incrementally to contact with the rough ground surface. The curves of normal reaction force versus normal displacement were fitted in a power-law function as follows:

$$f(x) = kx^n, \tag{3}$$

where k and n are coefficients determined by surface parameters including the surface topography and material properties.

3.3. Dynamic Model. Substituting the force-displacement equation (Equation (3)) into the kinetic equation of the TDOF system, the equation is obtained as follows:

Table 1: Nondimensional system parameters of the field experiment.

u	ω_s	n	ξ_1	ξ_2	r	Y	τ
3.0707	255.323	2.1	0.2321	1.0184	0.0016	0.3178	5016.5

$$\begin{cases} m_1\ddot{z}_1 + d_1(\dot{z}_1 - \dot{z}_2) + k_1(z_1 - z_2) = -F\sin(\omega t), \\ m_2\ddot{z}_2 + (d_1 + d_2)\dot{z}_2 - d_1\dot{z}_1 + k(z_2 + z_{s2})^n - F_t \\ \quad - k_1(z_1 - z_2) = F\sin(\omega t), \end{cases} \tag{4}$$

This is normalized using the following nondimensional variables:

$$\begin{aligned} x_1 &= \frac{z_1}{z_{s2}}, \\ x_2 &= \frac{z_2}{z_{s2}}, \\ z_{s2} &= \left(\frac{F_t}{k}\right)^{1/n}, \\ \omega_s &= \sqrt{\frac{nkz_{s2}^{n-1}}{m_2}}, \\ \tau &= \omega_s t, \\ \Omega &= \frac{\omega}{\omega_s}, \\ u &= \frac{m_1}{m_2}, \\ r &= \frac{k_1}{unkz_{s2}^{n-1}}, \\ \xi_1 &= \frac{c_1}{2m_1\omega_s}, \\ \xi_2 &= \frac{c_2}{2m_2\omega_s}, \\ Y &= \frac{F}{F_t}. \end{aligned} \tag{5}$$

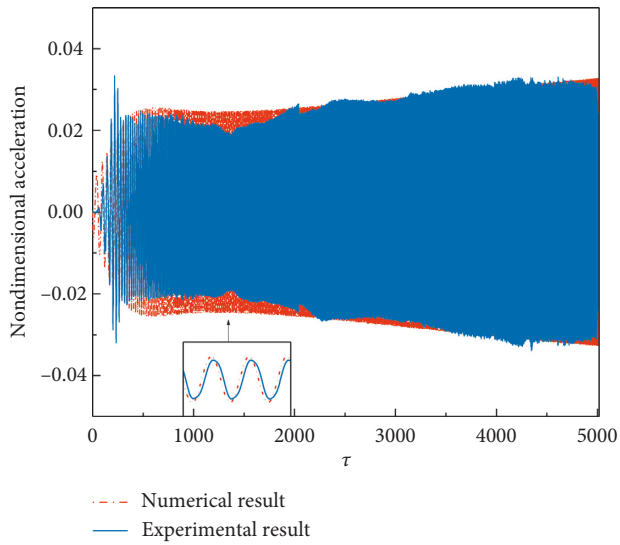

Figure 6: Comparison between the numerical and experimental results.

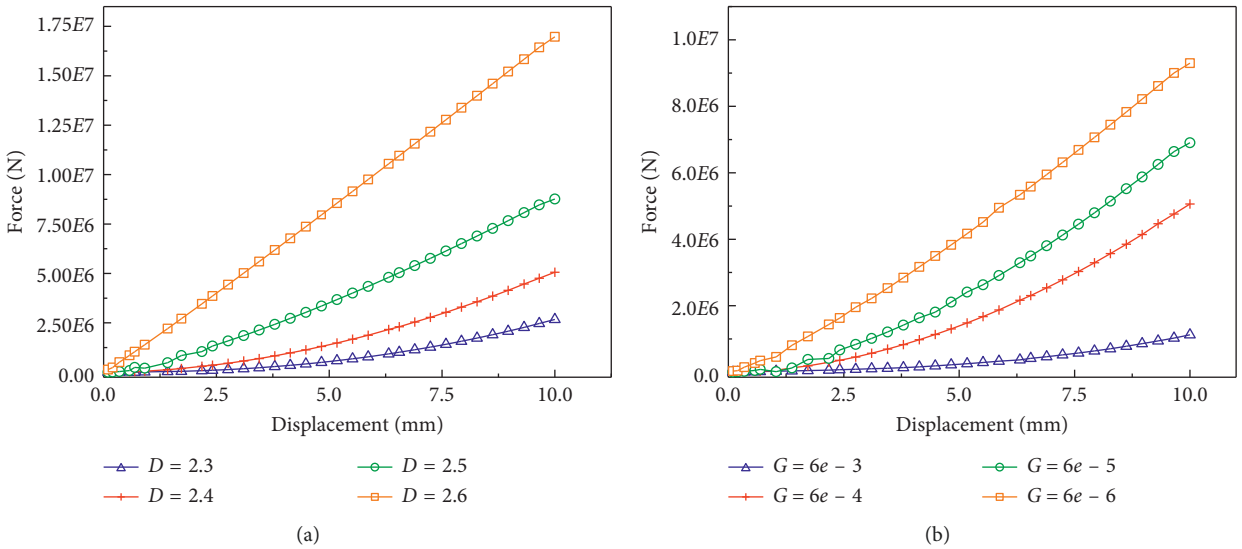

Figure 7: Normal contact reaction force versus displacement for contact interfaces with different fractal parameters: (a) fractal dimension D; (b) fractal roughness G.

Table 2: The k and n values for different fractal parameters.

D	G (mm)	k (N/mm^n)	n
2.3	$6e-4$	1.343e4	2.299
2.4	$6e-4$	6.885e4	1.868
2.5	$6e-4$	4.076e5	1.338
2.6	$6e-4$	1.534e6	1.046
2.4	$6e-3$	5.121e3	2.333
2.4	$6e-5$	1.564e5	1.653
2.4	$6e-6$	5.498e5	1.233

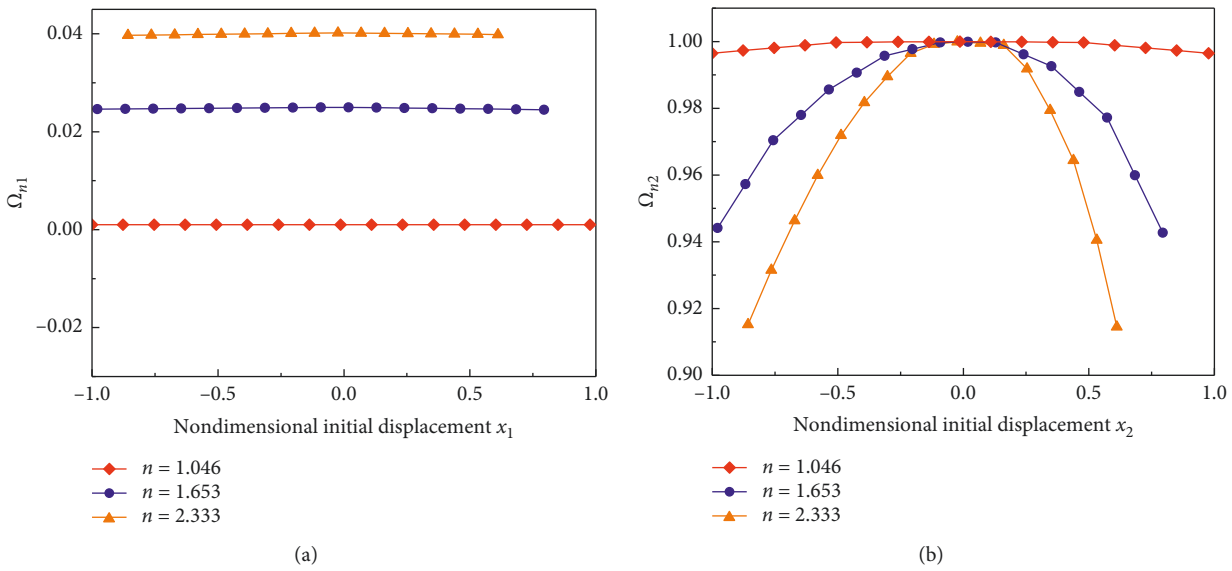

FIGURE 8: Nondimensional natural frequency for different values of initial displacement x_2: (a) first-order natural frequency; (b) second-order natural frequency.

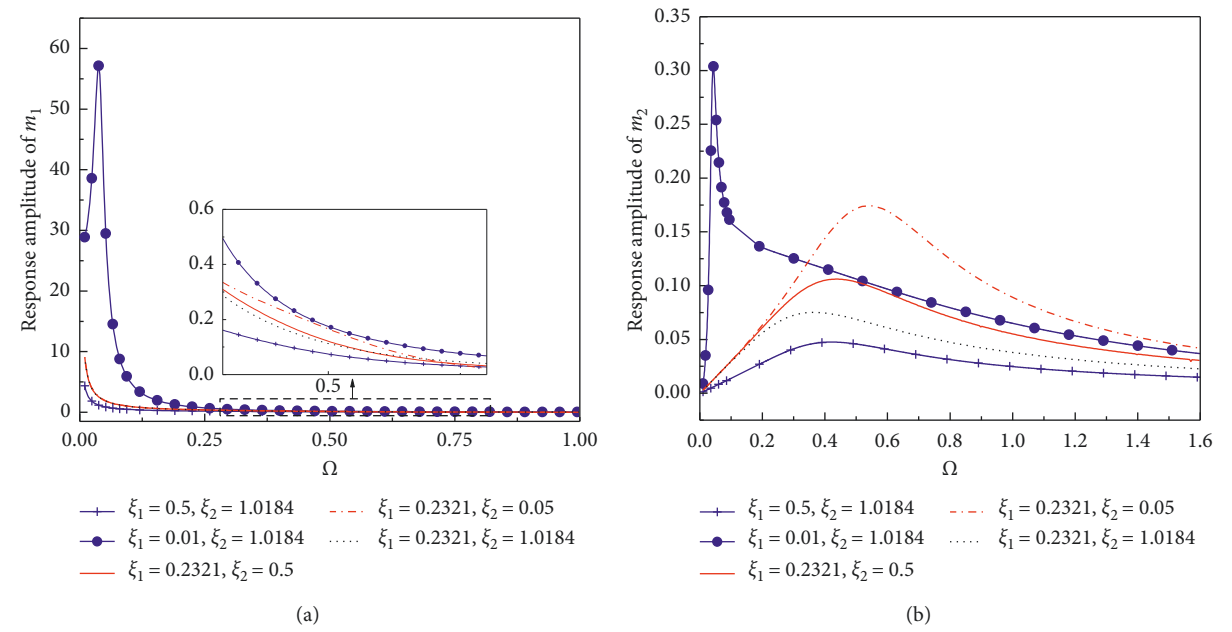

FIGURE 9: Effects of the damping parameters ξ_1 and ξ_2 on the frequency response curves: (a) response amplitude of reaction mass; (b) response amplitude of baseplate.

Equation (4) is expressed in a nondimensional form as

$$\begin{cases} \ddot{x}_1 + 2\xi_1(\dot{x}_1 - \dot{x}_2) + r(x_1 - x_2) = -\dfrac{1}{un} Y \sin(\Omega\tau), \\ \ddot{x}_2 + 2(u\xi_1 + \xi_2)\dot{x}_2 - 2u\xi_1\dot{x}_1 + \dfrac{1}{n}\left[(x_2 + 1)^n - 1\right] \\ \quad - ur(x_1 - x_2) = \dfrac{1}{n} Y \sin(\Omega\tau). \end{cases} \tag{6}$$

To simplify the nondimensional equation, the restoring force is approximated by a third-order Taylor series expansion, giving

$$\begin{cases} \ddot{x}_1 + 2\xi_1(\dot{x}_1 - \dot{x}_2) + r(x_1 - x_2) = -\dfrac{1}{un} Y \sin(\Omega\tau), \\ \ddot{x}_2 + 2(u\xi_1 + \xi_2)\dot{x}_2 - 2u\xi_1\dot{x}_1 + x_2 + \alpha_2 x_2^2 + \alpha_3 x_2^3 \\ \quad - ur(x_1 - x_2) = \dfrac{1}{n} Y \sin(\Omega\tau), \end{cases} \tag{7}$$

where $\alpha_2 = (n-1)/2$, $\alpha_3 = (n-1)(n-2)/6$.

Equation (7) can be solved numerically using the fourth-fifth order Runge–Kutta method to obtain the dynamic

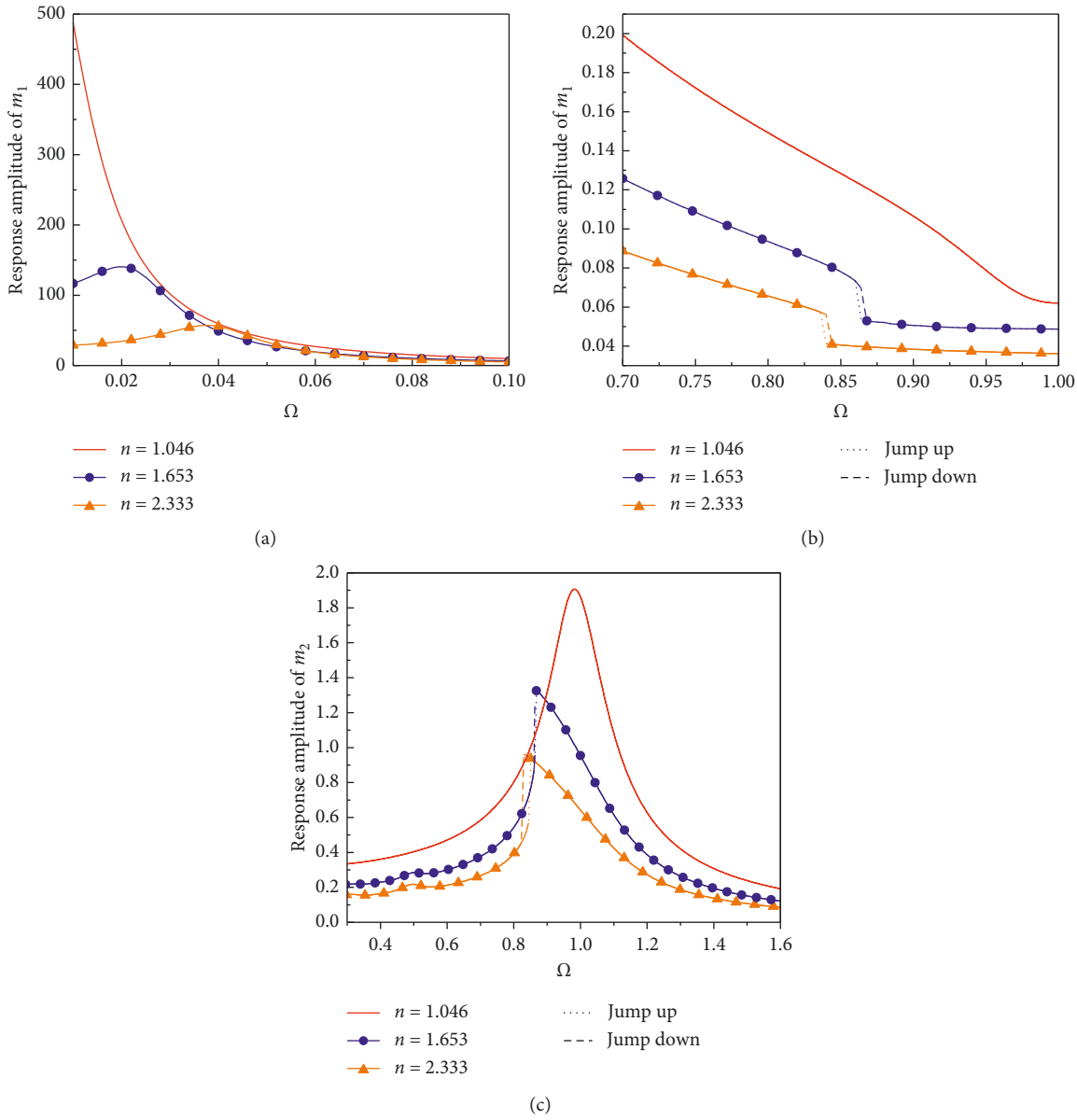

FIGURE 10: Frequency response curves for different rough surfaces: (a) resonance curves of the reaction mass; (b) response amplitude of the reaction mass; (c) response amplitude of the baseplate.

response of the TDOF system. To validate the dynamic model, a field experiment was developed in which the test vibrator was a 249 kN (55977 lbf) vibrator mounted on an EV56 seismic vibrator as shown in Figure 5(a). The acceleration of the reaction mass was obtained by an accelerometer located on the top of the reaction mass, as shown in Figure 5(b). As given in Table 1, the system parameters used for the following simulation were determined from the field experiment, which comprised a 5.905 t reaction mass, a 1.923 t baseplate, and 32.5 t vehicle. Furthermore, the test vibrator was operated under sweep excitation with a frequency of 3–120 Hz, and the excitation amplitude is 99,600 N. The profile of the test field ground surface on which the vibrator was located was measured by a three-dimensional laser scanner, and the parameter of Equation (3) for the test field ground surface was determined using the finite element model as above. The acceleration of the reaction mass calculated by Equation (7) is shown in Figure 6, along with the results measured by the accelerometer. From Figure 6, the numerical results clearly agree with the experimental results. Therefore, this vibrator-rough ground coupled model can be used in further research to study how the rough surface topography influences the dynamic response of the vibrator.

4. Results and Discussion

4.1. Force-Deflection Characteristics of Rough Surfaces. To establish the force-deflection characteristics of different rough grounds, different rough surface fractal parameters are chosen to construct different rough surface topographies. The fractal parameters are (i) $D = 2.3$, 2.4, 2.5, and 2.6 for $G = 6e-4$ m

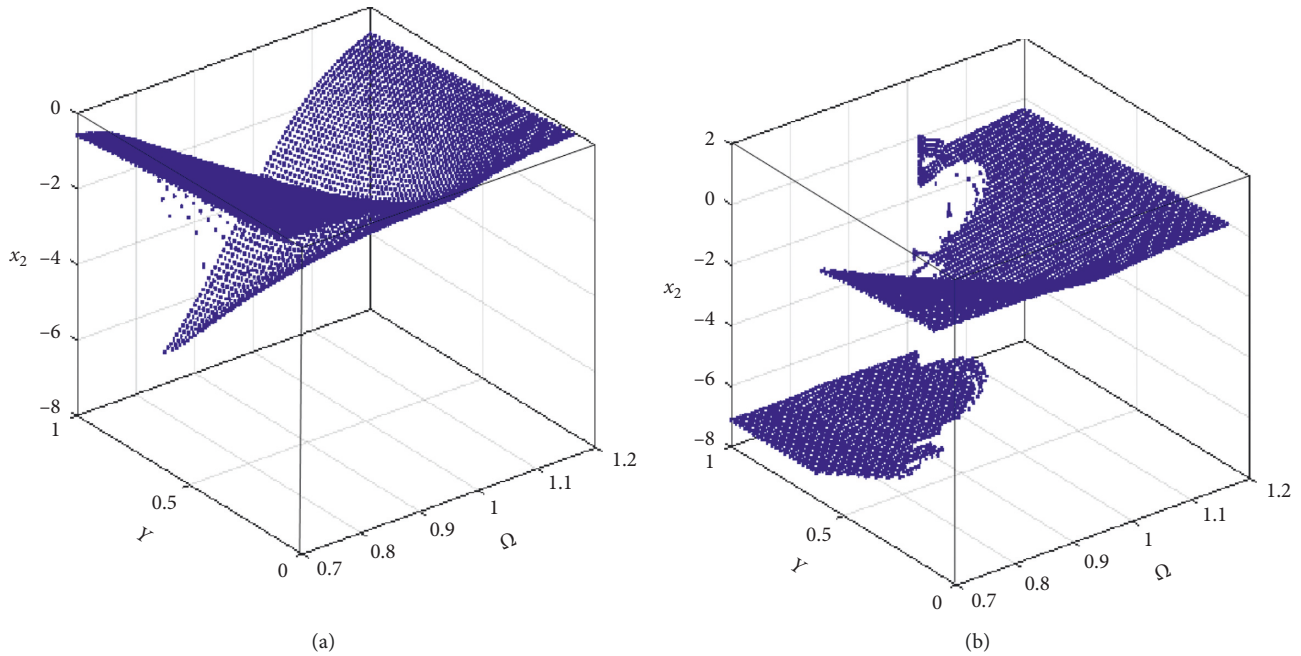

FIGURE 11: Bifurcation diagrams of the baseplate (with Ω and Y as control parameters) for different surface topographies: (a) $n = 1.046$; (b) $n = 2.333$.

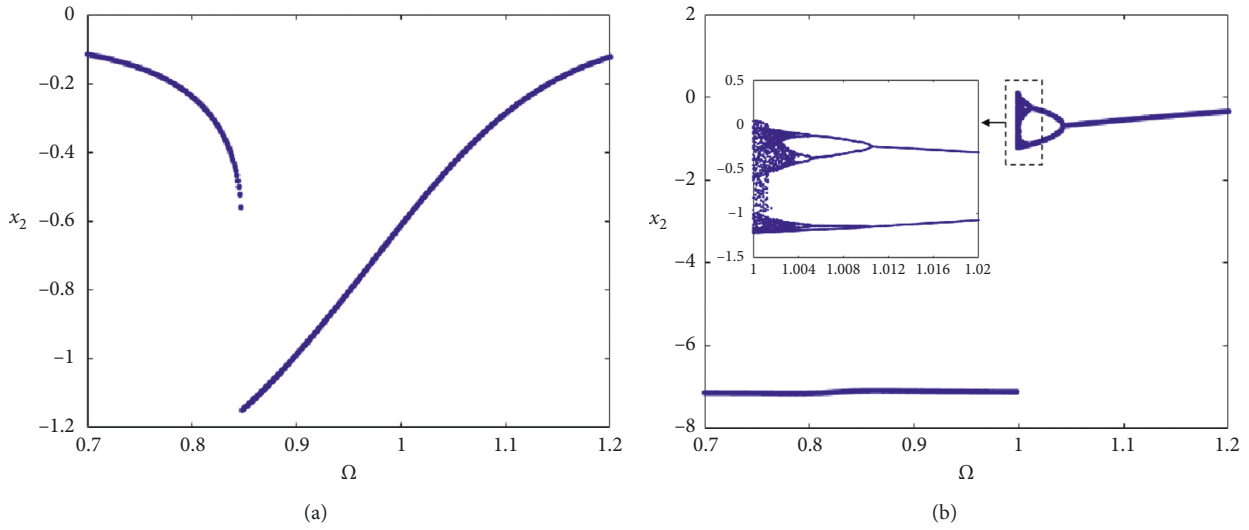

FIGURE 12: Cross sections of the three-dimensional bifurcation diagram for $n = 2.333$: (a) $Y = 0.3178$; (b) $Y = 0.943$.

and (ii) $G = 6e-3$ m, $6e-5$ m, and $6e-6$ m for $D = 2.4$. The elastic modulus of the baseplate pad is 2.12e5 MPa and that of the ground is 290 MPa. The equivalent elastic modulus E' ($1/E' = (1-\upsilon_1 2)/E_1 + (1-\upsilon_2 2)/E_2$) can be calculated, where E_1, E_2, υ_1, and υ_2 are elasticity modulus and Poisson's ratio of baseplate pad and ground, respectively [33]. The variations of the force-deflection characteristics for the different values of D and G are shown in Figure 7.

As can be seen in Figure 7, the rougher the surface topography (lower D and higher G), the stronger the nonlinearity, and vice versa. The values of k and n of Equation (3) for the different fractal parameters are given in Table 2. The value of n clearly increases with rougher ground surface topography.

4.2. Undamped Free Vibrations. The undamped free vibration of the TDOF system can be analyzed by setting the damping factor and excitation force to zero. Equation (7) then becomes

$$\begin{cases} \ddot{x}_1 + r(x_1 - x_2) = 0, \\ \ddot{x}_2 + x_2 + \alpha_2 x_2^2 + \alpha_3 x_2^3 - ur(x_1 - x_2) = 0. \end{cases} \tag{8}$$

Because of the nonlinear restoring forces among the contact interfaces, the initial displacement of the vibrator can affect the natural frequency of the system. The initial conditions are $x_1 = 0$, $\dot{x}_1 = 0$, and $\dot{x}_2 = 0$ for differing initial displacement x_2 of the baseplate. The nondimensional natural frequencies for differing initial displacement x_2

avoiding contact loss are calculated by using the fourth- and fifth-order Runge–Kutta method and are shown in Figure 8. The maximum initial displacement x_2 avoiding contact loss decreases with increasing n values, which corresponds to rougher contact interfaces. The maximum values of initial displacement x_2 in Figure 8 are 0.9771, 0.7946, and 0.6114 for $n = 1.046$, 1.653, and 2.333, respectively. It is noteworthy that the minimum values of initial displacement x_2 of the TDOF system differ from those of the SDOF system [21]. The minimum initial displacement of SDOF system for different contact interfaces is −1, while the range of minimum initial displacement x_2 is $x_2\,(\min) \le -1$. As can be seen from Figure 8(a), changing the initial displacement x_2 clearly has little influence on the first-order natural frequency of the system and mainly affects the second-order natural frequency under the present initial condition. The second-order natural frequency reaches the maximum value at the static equilibrium position and then decreases with the increase or decrease of the initial displacement from the static equilibrium position. In addition, the maximum reductions of the second-natural frequency are 8.54%, 5.66%, and 0.35% for $n = 1.046$, 1.653, and 2.333, respectively. According to the numerical results, it is inferred that the natural frequency of the baseplate decreases with the increase of the excitation force when the vibrator is in contact with rough ground surfaces. The result is similar to the research of Rik and Guy [34]. Meanwhile, the decrease rate of natural frequency for rougher ground surface is larger.

4.3. Harmonic Excited Vibration Results. To further understand how the rough contact interfaces influence the vibrator, the damped forced vibration characteristics of the system under external harmonic excitation are investigated. In order to obtain the effects of ξ_1 and ξ_2 on the frequency response of the system, several groups of various ξ_1 and ξ_2 values are used and the other system parameters are taken as above. Figure 9 shows the frequency response curves of the reaction mass and baseplate for different combinations of ξ_1 and ξ_2. It can be seen that ξ_1 and ξ_2 have obvious effects on the amplitude reduction of the reaction mass and baseplate especially the peak amplitude. Therefore, in the following study, ξ_1 and ξ_2 are taken as $\xi_1 = 0.01$ and $\xi_2 = 0.05$ to reduce the suppression of nonlinearity of the system.

Figure 10 compares the forced damped characteristics for different values of n. It can be observed that, with increasing n, which corresponds to rougher surface topography, the amplitudes of the reaction mass and baseplate decrease. The frequency response curves of the baseplate exhibit a jump phenomenon for $n = 1.653$ and 2.333, as do the frequency curves of the reaction mass at the same frequencies. However, there is no jump phenomenon observed in the resonance curves of the reaction mass. With the increase of the roughness of the surface topographies, the jump frequencies decrease as well as the hysteretic region between the jump-up and jump-down frequencies. It can also be observed that the frequency response curves for $n = 1.653$ and 2.333 bend to the left, the system exhibiting softening-spring-type behavior. Hence, when the vibrator is in contact with rough ground surface, due to the sweep excitation, the displacement response amplitude of the baseplate may jump to a larger value suddenly at the same drive level.

In the following section, the nondimensional frequency Ω and nondimensional excitation Y are taken as bifurcation parameters to obtain the bifurcation diagram of the baseplate in contact with the rough surface. The other parameters of the system are taken as $u = 3.0707$, $r = 0.0016$, $\xi_1 = 0.01$, and $\xi_2 = 0.05$. Figure 11 shows that, with increasing nondimensional excitation Y, the motion of the baseplate becomes more complicated. Therefore, the nondimensional excitation Y can affect the nonlinear oscillations of the coupled vibrator-rough ground system.

Cross sections of the three-dimensional bifurcation diagram for $n = 2.333$ are shown in Figure 12. For $Y = 0.3178$, the motion of the system is periodic for $\Omega < 0.847$ (approximately), then the system response jumps to another period motion. When $Y = 0.943$, the motion of the system is a periodic motion before about $\Omega < 1$. At $\Omega = 1$, the system enters chaotic motion, after which it returns to periodic motion through period-doubling bifurcation. Therefore, the system exhibits period-doubling bifurcations. Based on the bifurcation diagrams, the relative Poincaré map and power spectrum are shown in Figures 13–18, where (a) and (b) depict the Poincaré map on plane $(x_2, \dot{x}_2)$ and the power spectrum, respectively. Poincaré map and power spectrum are efficient ways to distinguish the periodic motions and chaotic motions. At $\Omega = 0.8$ (Figure 13), period-1 motion is mainly based on the fundamental frequency vibration with the same frequency as the excitation, accompanied by high-order harmonics. Figure 14 shows that the Poincaré map has the appearance of a strange attractor typical of chaos, and the spectrum is a continuous curve. Then, the system turns into a period-8 response at $\Omega = 1.006$ (Figure 15). The Poincaré map has eight points, and the spectrum has 1/8 subharmonic. With the increase of the exciting frequency, the eight points combine into four points, and then four points combine into two points (Figures 16 and 17). The spectrum has 1/4 subharmonic and 1/2 subharmonic as $\Omega = 1.01$, 1.02, respectively. After $\Omega = 1.1$ (Figure 18), the system enters into a periodic motion. According to the above results, the vibrator system may exhibit bifurcation and chaotic motion under high drive level. These motions will affect the accuracy of vibrator output signal. Using multiple seismic vibrators to work at the same time rather than one seismic vibrator under high drive level is an efficient way to avoid chaotic motion.

5. Conclusions

Herein, the influence of the rough contact interfaces on a TDOF coupled vibrator-rough ground system was studied. The main conclusions are as follows:

(1) The force-deflection characteristic of the contact interfaces between the vibrator and ground was determined by finite element analysis according to the fractal contact model. The restoring force of the nonlinear contact interfaces was described using a

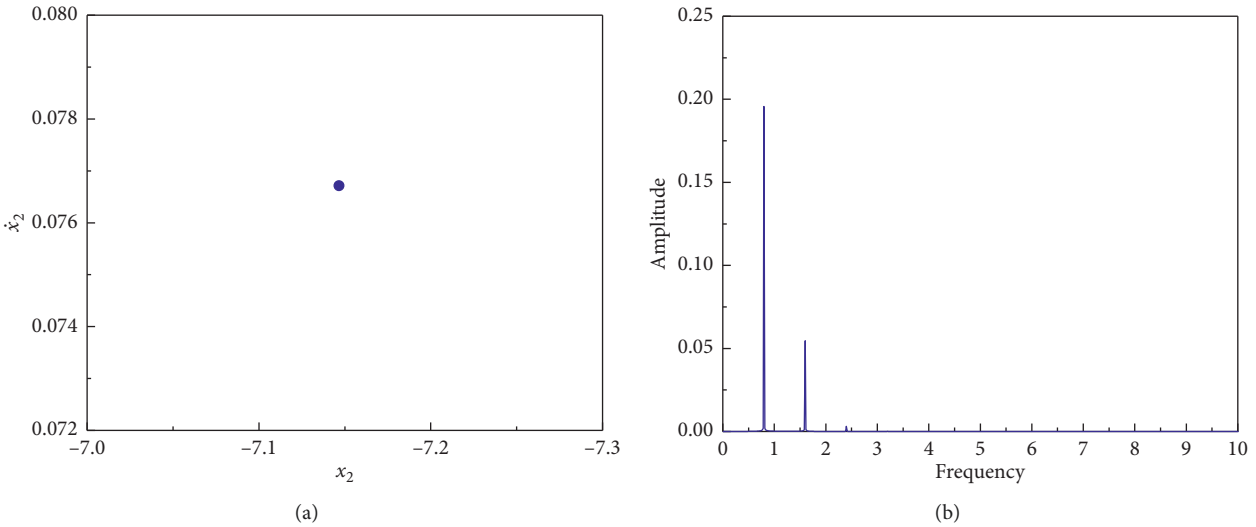

Figure 13: Period-1 motion of the baseplate for $\Omega = 0.8$.

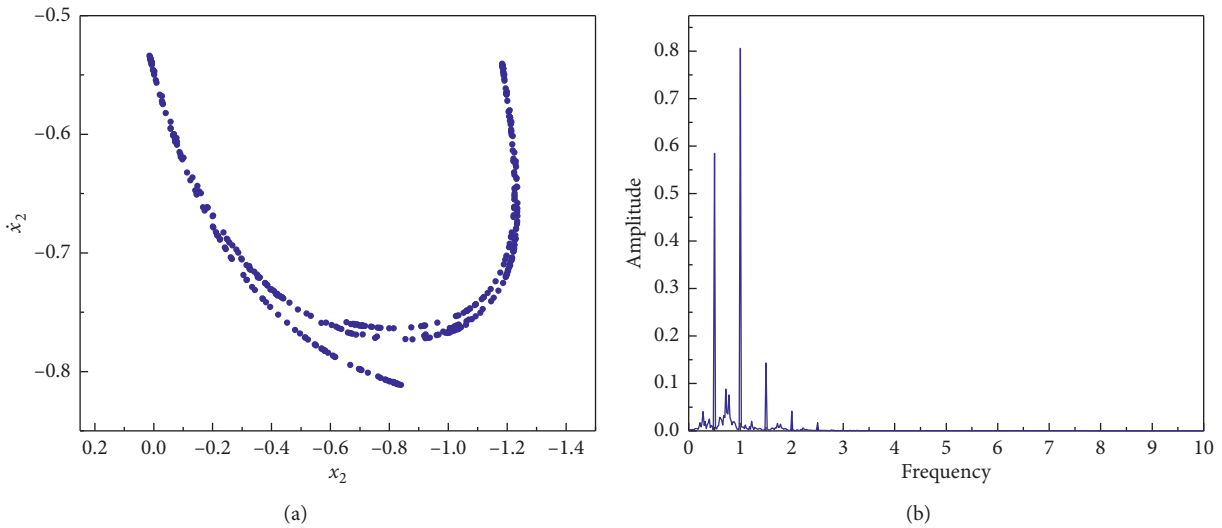

Figure 14: Chaotic motion of the baseplate for $\Omega = 1.001$.

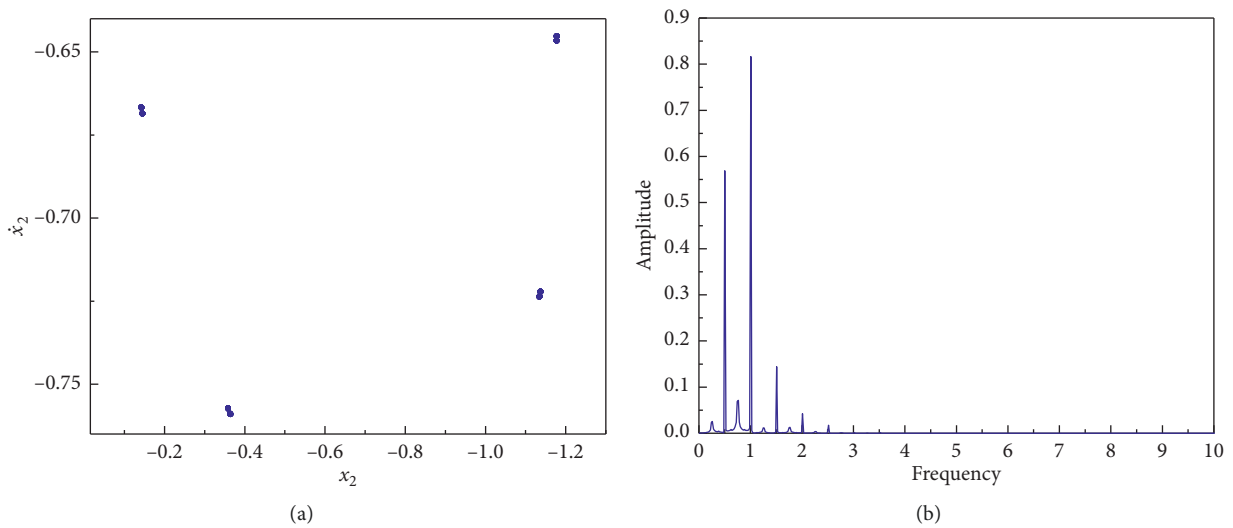

Figure 15: Period-8 motion of the baseplate for $\Omega = 1.006$.

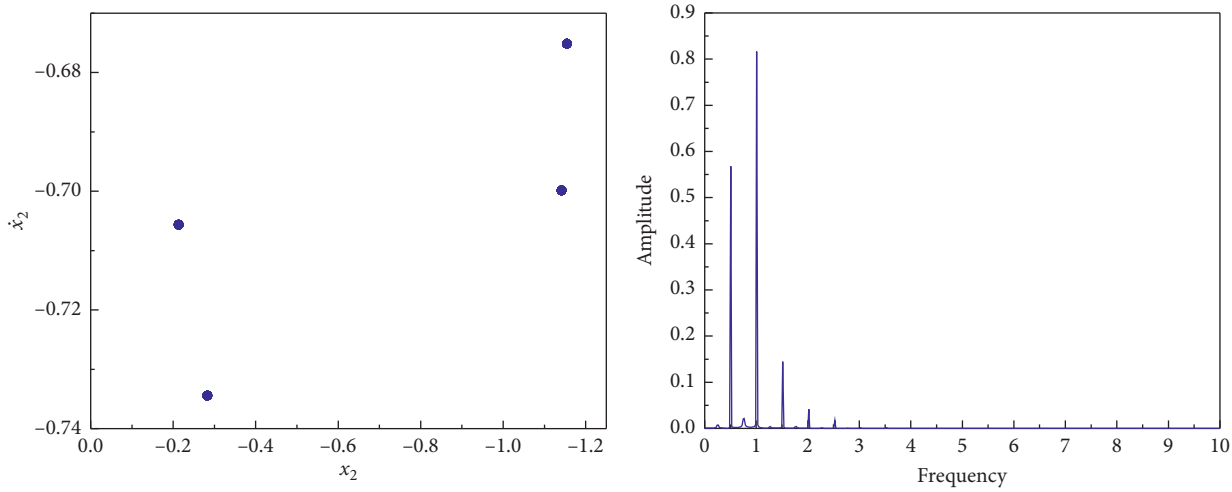

Figure 16: Period-4 motion of the baseplate for $\Omega = 1.01$.

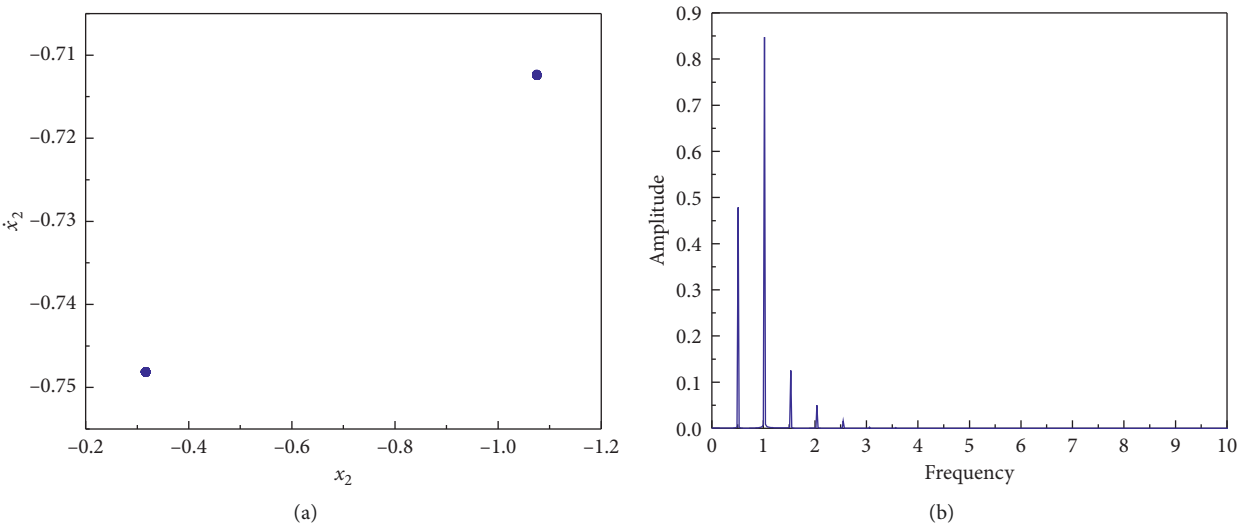

Figure 17: Period-2 motion of the baseplate for $\Omega = 1.02$.

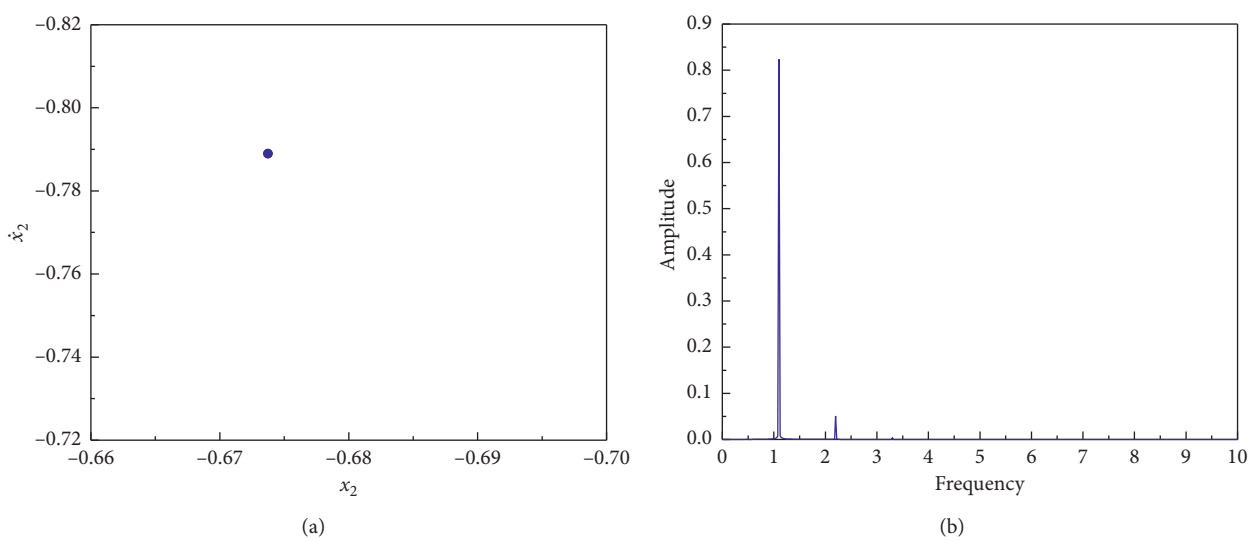

Figure 18: Period-1 motion of the baseplate for $\Omega = 1.1$.

power-law function that depends on the finite element analysis results.

(2) With the increase or decrease of the initial displacement, the second-order natural frequency of the system decreases and the reduction of the second-order natural frequency increases with rougher contact interfaces. However, the initial displacement has little influence on the first-order natural frequency of the system.

(3) The harmonic response analysis shows that the jump phenomenon occurs in the amplitude curves of the reaction mass and baseplate at the same frequencies. The jump frequencies and the response amplitude of the system both decrease with rougher contact interfaces. According to the three-dimensional bifurcation diagram, it is inferred that larger nondimensional excitation can cause the chaotic motions of the system with rough contact interfaces. It is found that, when a vibrator is used on rougher ground surface, it is not suitable to use excessive excitation force.

Data Availability

The numerical data used to support the findings of this study are available from the corresponding author upon request.

Conflicts of Interest

The authors declare that there are no conflicts of interest regarding the publication of this article.

Acknowledgments

This work was supported by the National Science Foundation of China (Grant nos. 50474040 and 50674078) and the National High Technology Research and Development Program of China (Grant no. 2012AA061201).

References

[1] K. L. Johnson, *Contact Mechanics*, Cambridge University Press, Cambridge, UK, 1985.

[2] O. E. Lundberg, A. Nordborg, and I. Lopez Arteaga, "The influence of surface roughness on the contact stiffness and the contact filter effect in nonlinear wheel-track interaction," *Journal of Sound and Vibration*, vol. 366, pp. 429–446, 2016.

[3] I. I. Argatov and Y. A. Fadin, "Mathematical modeling of the periodic wear process in elastic contact between two bodies," *Journal of Friction and Wear*, vol. 29, no. 2, pp. 81–85, 2008.

[4] B. Mandelbrot, "How long is the coast of britain? Statistical self-similarity and fractional dimension," *Science*, vol. 156, no. 3775, pp. 636–638, 1967.

[5] B. B. Mandelbrot, *The Fractal Geometry of Nature*, W.H. Freeman, New York, NY, USA, 1982.

[6] M. V. Berry and Z. V. Lewis, "On the weierstrass-mandelbrot fractal function," in *Proceedings of the Royal Society A: Mathematical, Physical and Engineering Sciences*, vol. 370, no. 1743, pp. 459–484, 1980.

[7] A. Majumdar and B. Bhushan, "Role of fractal geometry in roughness characterization and contact mechanics of surfaces," *Journal of Tribology*, vol. 112, no. 2, pp. 205–215, 1990.

[8] M. Ciavarella and G. Demelio, "Elastic multiscale contact of rough surfaces: archard's model revisited and comparisons with modern fractal models," *Journal of Applied Mechanics*, vol. 68, no. 3, pp. 496–498, 2001.

[9] W. Yan and K. Komvopoulos, "Contact analysis of elastic-plastic fractal surfaces," *Journal of Applied Physics*, vol. 84, no. 7, pp. 3617–3624, 1998.

[10] S. Jiang, Y. Zheng, and H. Zhu, "A contact stiffness model of machined plane joint based on fractal theory," *Journal of Tribology*, vol. 132, article 011401, 2010.

[11] X. Miao and X. Huang, "A complete contact model of a fractal rough surface," *Wear*, vol. 309, no. 1-2, pp. 146–151, 2014.

[12] P. Liu, H. Zhao, K. Huang, and Q. Chen, "Research on normal contact stiffness of rough surface considering friction based on fractal theory," *Applied Surface Science*, vol. 349, pp. 43–48, 2015.

[13] K. Komvopoulos and N. Ye, "Elastic-plastic finite element analysis for the head-disk interface with fractal topography description," *Journal of Tribology*, vol. 124, no. 4, pp. 775–784, 2002.

[14] L. Pei, S. Hyun, J. Molinari, and M. Robbins, "Finite element modeling of elasto-plastic contact between rough surfaces," *Journal of the Mechanics and Physics of Solids*, vol. 53, no. 11, pp. 2385–2409, 2005.

[15] N. Ghosh and P. Sahoo, "Finite element contact analysis of fractal surfaces," *Journal of Physics D*, vol. 40, pp. 4245–4252, 2007.

[16] P. R. Nayak, "Contact vibrations," *Journal of Sound and Vibration*, vol. 22, pp. 297–322, 1972.

[17] J. Sabot, P. Krempf, and C. Janolin, "Non-linear vibrations of a sphere-plane contact excited by a normal load," *Journal of Sound and Vibration*, vol. 214, no. 2, pp. 359–375, 1998.

[18] Q. L. Ma, A. Kahraman, J. Perret-Liaudet, and E. Rigaud, "An investigation of steady-state dynamic response of a sphere-plane contact interface with contact loss," *Journal of Applied Mechanics*, vol. 74, no. 2, pp. 249–255, 2007.

[19] J. Perret-Liaudet and E. Rigaud, "Experiments and numerical results on non-linear vibrations of an impacting Hertzian contact. Part 2: random excitation," *Journal of Sound and Vibration*, vol. 265, no. 2, pp. 309–327, 2003.

[20] H. Xiao, M. J. Brennan, and Y. Shao, "On the undamped free vibration of a mass interacting with a Hertzian contact stiffness," *Mechanics Research Communications*, vol. 38, no. 8, pp. 560–564, 2011.

[21] H. Xiao, Y. Shao, and M. J. Brennan, "On the contact stiffness and nonlinear vibration of an elastic body with a rough surface in contact with a rigid flat surface," *European Journal of Mechanics-A/Solids*, vol. 49, pp. 321–328, 2015.

[22] T. Jana, A. Mitra, and P. Sahoo, "Dynamic contact interactions of fractal surfaces," *Applied Surface Science*, vol. 392, pp. 872–882, 2017.

[23] A. D. Dimarogonas and S. Haddad, *Vibration for Engineers*, Prentice-Hall, Englewood Cliffs, NJ, USA, 1992.

[24] L. Cveticanin, "The motion of a two-mass system with non-linear connection," *Journal of Sound and Vibration*, vol. 252, no. 2, pp. 361–369, 2002.

[25] A. F. Vakakis and R. H. Rand, "Non-linear dynamics of a system of coupled oscillators with essential stiffness non-linearities," *International Journal of Non-Linear Mechanics*, vol. 39, no. 7, pp. 1079–1091, 2004.

[26] C. Alain and M. Laycock, "Vibrator controlling system," U.S. Patent 3208550, 1965.
[27] J. J. Sallas, "Seismic vibrator control and the downgoing P-wave," *Geophysics*, vol. 49, no. 6, pp. 732–740, 1984.
[28] A. V. Lebedev and I. A. Beresnev, "Nonlinear distortion of signals radiated by vibroseis sources," *Geophysics*, vol. 69, no. 4, pp. 968–977, 2004.
[29] J. Liu, Z. Q. Huang, and G. Li, "Dynamic characteristics analysis of a seismic vibrator-ground coupling system," *Shock and Vibration*, vol. 2017, Article ID 2670218, 12 pages, 2017.
[30] A. C. Armstrong, "On the fractal dimensions of some transient soil properties," *European Journal of Soil Science*, vol. 37, pp. 641–652, 2010.
[31] Z. F. Hou, Z. Chen, and L. Li, "Fractal analysis of soil profile roughness," *Advanced Materials Research*, vol. 383–390, pp. 4944–4948, 2012.
[32] A. Majumdar and C. L. Tien, "Fractal characterization and simulation of rough surfaces," *Wear*, vol. 136, no. 2, pp. 313–327, 1990.
[33] S. Jiang, Y. Zheng, and H. Zhu, "A contact stiffness model of machined plane joint based on fractal theory," *Journal of Topology*, vol. 132, no. 1, 2010.
[34] R. Noorlandt and G. Drijkoningen, "On the mechanical vibrator-earth contact geometry and its dynamics," *Geophysics*, vol. 81, no. 3, pp. 23–31, 2016.